ELSEVIER

Ultramicroscopy 82 (2000) 193–202

ultramicroscopy

www.elsevier.nl/locate/ultramic

Quantitative interrogation of micropatterned biomolecules by surface force microscopy

Michael D. Garrison*, Todd C. McDevitt, Reto Luginbühl, Cecilia M. Giachelli, Pat Stayton, Buddy D. Ratner

University of Washington Engineered Biomaterials and Department of Bioengineering, University of Washington, Seattle, WA 98195-1750, USA

Received 31 May 1999; received in revised form 20 August 1999

Abstract

Synthetic biomaterials are widely used in medical implants with success in improving and extending quality of life. However, these materials were not originally designed to interact with cells through specific signaling pathways. As a result, the interaction with the body is mediated through passive adsorption of a disorganized protein monolayer. Next generation biomaterials have been proposed to be active in modifying the biological response of the host through the incorporation of specific biorecognition moieties. An important tool in the development of these novel active biomaterials is the scanning force microscope (SFM). The SFM allows for interrogation of bioactive biomaterials in mapping or spectroscopic modes. In this work, micropatterned protein surfaces were prepared using biomolecules implicated in wound healing. The surfaces were imaged via SFM and the specific binding forces between surface associated biomolecules and antibody functionalized tips were quantified.

PACS: 07.79; 87.64; 36.20; 87.15

Keywords: Scanning force microscopy; Microcontact printing; Osteopontin; Biomaterials

1. Introduction

Synthetic biomaterials save lives, improve patient care, and extend the quality of life for millions of people each year. However, even these successful biomaterials do not integrate naturally with the host. Rather, these metals, ceramics, and polymers are walled off via a thin, quiescent collagenous capsule, irrespective of their widely different surface properties. In most cases, the collagenous capsule acts to passivate the wound site and is deemed "biocompatible", but in many important cases (e.g. implantable sensors) the material's function is adversely impacted [1].

All biomaterials are immediately coated with an adsorbed layer of proteins upon exposure to body fluids (Fig. 1). This protein layer is disorganized and multi-component, with each adsorbed protein

* Corresponding author. Present address: Roche Diagnostic Corporation, Indianapolis, IN 46250-0457, USA. Tel.: + 1-317-576-7551; fax: + 1-317-576-2236.

E-mail address: michael.garrison@roche.com (M.D. Garrison)

0304-3991/00/$ - see front matter
PII: S0304-3991(99)00150-3

having multiple conformations and orientations on the surface. We have hypothesized that mis-recognition of this disorganized adsorbed protein layer by surrounding cells leads to the classic foreign body reaction and device encapsulation [2]. However, normal wound healing in the body involves a coordinated symphony of specific molecular recognition and cellular biochemical processes to repair, remodel, revascularize, and regenerate the damaged tissue. More normal wound healing has been observed recently in the presence of implanted biomaterials [3,4]. These observations indicate that the biochemical pathways controlling the foreign body reaction may be attenuated, and the pathways leading to normal healing activated. The next generation of biomaterials, "Engineered Biomaterials", will incorporate the appropriate specific signaling agents at the host interface to direct the biological response [5,6].

In order to facilitate the development of this next generation of biomaterials, new enabling technologies must be developed. One area of need is the means to spatially image and functionally characterize the surface presentation of biospecific signaling moieties on a biomaterial. This is a challenging task, as these molecules are typically only a few nm^3 in size, operate in biological (aqueous) environments, and act through a spatial array of non-covalent interactions leading to recognition events [7,8]. Typically, such binding events are relatively weak and reversible. These criteria challenge most conventional surface analytical techniques.

The SFM is an attractive platform for development into a recognition imaging tool [9–14]. This technique exhibits the lateral resolution necessary to detect individual molecules, is compatible with aqueous environments, and operates through force transduction allowing for the detection and quantification of intermolecular forces of > 10 pN. The SFM has been used to monitor specific molecular recognition events in ligand/receptor [11,12,15,16], antibody/antigen [13,17,18], and DNA base pair binding [19,20]. Some recent studies have also described the use of SFM to spatially map surfaces with specific intermolecular recognition forces used as the agent of image contrast [19,21–23]. As a result, the SFM appears to be uniquely well suited for application to engineered biomaterial surfaces (Fig. 2).

Arrangement of biological signaling agents on a surface with spatial precision and fidelity has recently been advanced through the implementation of microcontact printing (μCP) [24–26]. This approach utilizes an elastomeric template to transfer the protein molecules to the surface of interest through direct surface–surface contact printing. The attractiveness of this technique lies in the versatility and ease in preparing surface protein patterns.

In this study, we describe the application of SFM to quantitatively interrogate micropatterned biomolecules. Accurate quantitation of the recognition forces is necessary for comparison of multiple surface preparations. Micropatterning was employed to engineer a control region onto the surface to facilitate visualization of the recognition processes. The biomolecule of interest in this study was osteopontin (OPN) a protein identified as playing an important role in bone remodeling, implant calcification and wound healing [27–29]. Our results indicate that (1) OPN patterns may be engineered on surfaces for interrogation via SFM, (2) antibody recognition of the patterned OPN may be visualized via SFM, (3) binding forces between OPN and OPN antibody are quantitatively distinct from the control surface regions.

2. Materials and methods

2.1. Materials

Silicon (Silicon Quest Intl.), glass microscope slides (VWR Scientific), glass coverslips (Carolina Biologicals), mica (SPI Supplies), filler-free poly(dimethyl siloxane) (PDMS, Sylgard 187, Dow Corning), photoresist (AZ1512) and developer (AZ351) (Shipley Inc.), *n*-octadecyltrichloro silane (OTS), *n*-2-aminoethyl-3-aminopropyltrimethoxy silane (EDS) (Gelest Inc.), benzophenone-isothiocyanate (BZP-ITC, Molecular Probes). Bovine serum albumin (BSA), human serum albumin (HSA), rabbit-anti-BSA (α-BSA) (Sigma Chemical Co.). Fluorescein labeled mouse-anti-goat antibody (α-Goat) (Pierce) Recombinant rat osteopontin (OPN) and goat-anti-rat osteopontin antibody

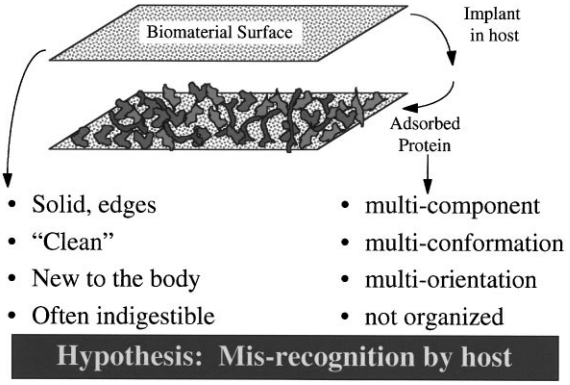

Fig. 1. Schematic representation of the biomaterial interface. A generic biomaterial adsorbing a layer of protein upon implantation. It is hypothesized that mis-recognition of this disorganized protein layer by the host cells leads to an alternative pathway of healing response termed the foreign body reaction and eventual encapsulation of the implant.

(α-OPN) were produced in house as previously described [30]. All solvents and buffers were of reagent grade or better and obtained from commercial sources. All water used was purified to $R = 18\ \mathrm{M}\Omega$ (ModuLab, US Filter).

2.2. *Microcontact printing* (μ*CP*)

Photoresist patterns were designed on silicon wafer substrates via conventional optical microlithographic techniques. The patterned silicon substrate was silanized by vapor-phase reaction in a vacuum dessicator with OTS for 30 min. A 10 : 1 (resin : crosslinker) mixture of PDMS was applied to the photoresist pattern and cured in place overnight at 60°C. The PDMS stamps were subsequently removed from the substrate and rinsed with 100% ethanol and ultrapure water. Protein solutions (specific concentrations described in the text below) were applied to the stamp in 100 μl volumes for 30–60 min, after which time the residual solution was removed via pipette aspiration and the stamps sequentially rinsed 3× in buffer, 3× in ultrapure water, and then dried by gentle blowing with a stream of prepurified nitrogen. The stamps were then brought into contact with the substrate of interest such that optical contact was observed. The contact time was kept constant at 1 min. Following removal of the stamp, the newly patterned surfaces were either mounted for imaging, or removed for secondary labeling.

2.3. *Tip functionalization*

Diced silicon chips and commercially available SFM cantilevers with integrated probe tips (Digital Instruments, standard NP, silicon nitride tips) were cleaned via solvent washing in acetone and methanol, followed by exposure to UV/ozone cleaning for 15 min. Upon removal from the ozone cleaner, the samples were immersed for 1 min in Piranha

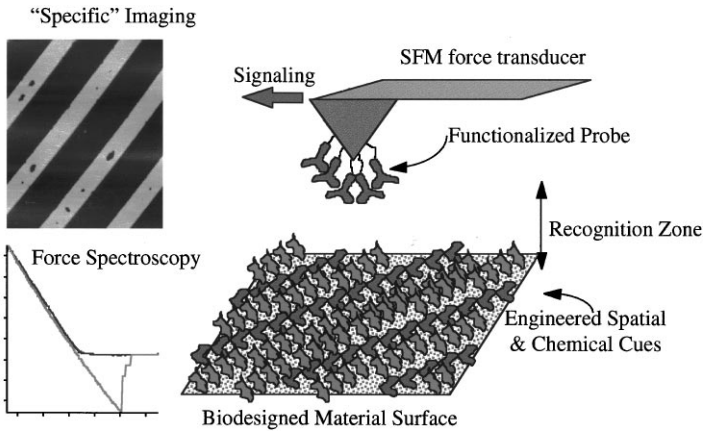

Fig. 2. Schematic reprsentation of a recognition imaging system for engineered biomaterials research. Using the force transduction capabilities of the SFM, functionalized probe tips may be used to quantitatively interrogate engineered surfaces with discrete force spectroscopy or lateral mapping.

solution (4 : 1 H_2SO_4 : H_2O_2, 100°C, note that this procedure is highly dangerous and appropriate personal protective equipment should be used during handling). The samples were then exhaustively rinsed in copious amounts of ultrapure water, dried under a circulating nitrogen atmosphere and placed in a vacuum oven at 60°C overnight. The samples were then aminated via vapor phase (15 min, 100°C, saturated atmosphere) or liquid phase (1% w/v in anhydrous hexane, 5 min, 25°C) silanization with EDS. The reaction was quenched by rinsing in excess solvent and the silane films cured in a vacuum oven overnight at 60°C. Aminated tips were then immersed in 5 ml of pH 9.0 sodium bicarbonate buffer solution saturated against 100 μl of 0.1 mg/ml BZP-ITC in DMSO. The isothiocyanate was allowed to couple to the ethylenediamine for 1 h, after which the tips were rinsed with copious amounts of ultrapure water and then re-equilibrated against pH 7.4 PBS. α-OPN (10 μg/ml in PBS) was injected into the tip reaction vessel, and allowed to adsorb for 1 h. The tips were then irradiated in situ for 15 min ($\lambda_{ex} = 365$ nm, UVGL-25, UVP Co.), triply rinsed in PBS and ultrapure water, photochemically crosslinking the adsorbed biomolecules to the tip surface.

2.4. SFM

SFM was performed using a NanoScope II instrument (Digital Instruments) with an attached digital storage oscilloscope (TDS 520A Tektronics, Inc.). For imaging of protein patterns with unfunctionalized tips, cleaned triangular cantilevers with oxide-sharpened Si_3N_4 tips (DI) or silicon tips were used (NTMDT Inc., KTek). When necessary, the cantilever spring constant was measured via the "thermal noise" method [31]. To accurately employ this method with the NanoScope II, it was necessary to temporarily alter the bandwidth of the microscope during data acquisition [32]. The bandwidth was returned to the manufacturer's settings for all force curve and imaging applications. For the force curves presented in this work, the calibrated force constant was $k_{cant} = 0.013$ nN/nm. Tip–sample forces were minimized ($\leqslant 10$ nN), and scan rates held below 2.5 Hz. SFM data was obtained under ambient conditions (RH ≈ 40–50%, $T \approx 20$–25°C), or in aqueous solution using a fluid cell. Raw images were flattened to correct for non-linear curvature of the sample stage piezo-tube response. Roughness values and surface feature dimensions were calculated using the manufacturer's provided software. Force curves were measured by collection via the digital storage oscilloscope of the photodiode output and z-piezo drive signal. Using the calibration obtained from the cantilever, the force curve data was analyzed using Igor Pro (Wavemetrics Inc.). Image presentation was performed using ImageSXM (Dr. Steve Barrett).

2.5. Fluorescence microscopy

Fluorescence microscopy of microcontact printed protein arrays and protein conjugated SFM tips was performed on a Nikon Diaphot inverted microscope (Nikon) equipped with a water-cooled CCD camera (Photometrics, LTD.). Images were acquired using Metamorph image analysis software (Universal Imaging Corp.), through a standard FITC filter set (XF23, Omega Optical).

2.6. Electron spectroscopy for chemical analysis (ESCA)

ESCA was performed on a Surface Science Instruments (SSI) S-Probe ESCA instrument. A take-off angle of 55° was used to collect compositional and high-resolution data from the uppermost 60 Å of the surface. SSI data analysis software was used (1) to calculate the elemental compositions from the peak areas and (2) to peak fit the high-resolution spectra. Elemental compositions are reported in atomic percent.

3. Results and discussion

The ability to micropattern biomolecules was first established through the use of a robust model protein, BSA. Fig. 3 displays μCP BSA on a freshly cleaved mica substrate. The mica lattice may be visualized in the intermediate regions, establishing this substrate as the reference region. The BSA

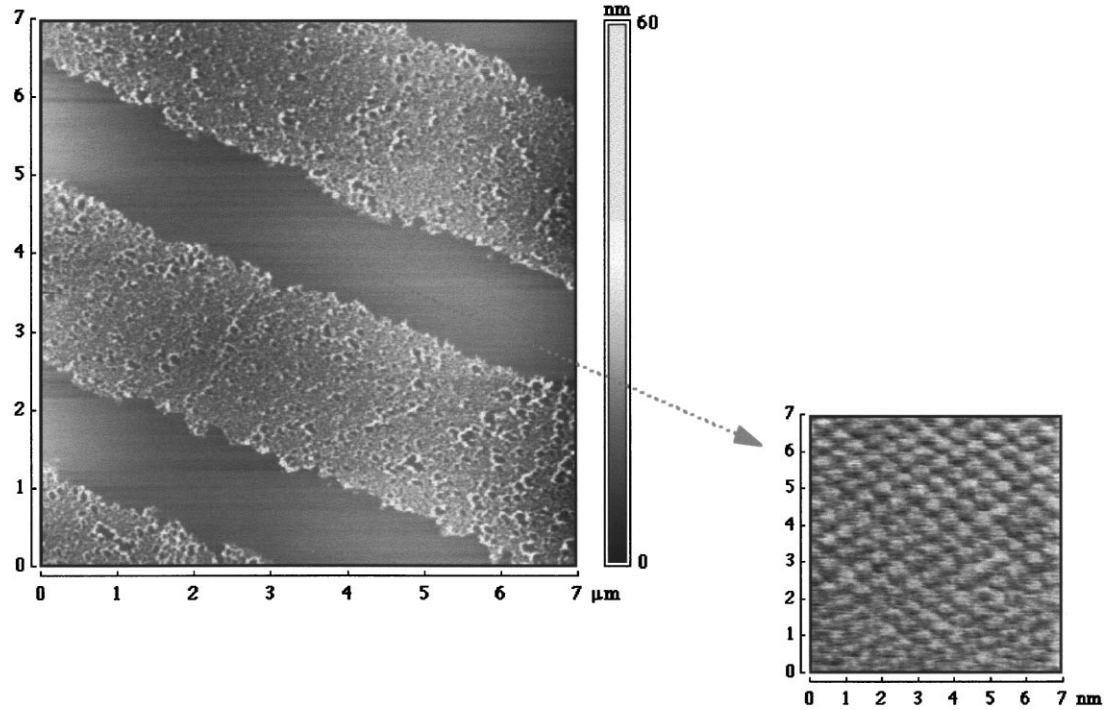

Fig. 3. SFM image of a 2 μm μCP line pattern of bovine serum albumin (BSA) on mica. Contact time of 1 min, 100 μg/ml BSA in PBS inking solution. Imaged in air with an oxide sharpened tip. Inset of mica lattice imaged in intermediate lane.

lanes are slightly wider than the expected 2 μm, due to compression of the PDMS under the increased normal load during stamping required to maintain uniform optical contact. The height of the lanes is 3.5–4.5 nm, in good agreement with the molecular dimensions of BSA ($40 \times 40 \times 120$ Å) assuming that the molecule is aligned with the long axis parallel to the surface.

The protein pattern is non-uniform, with numerous defect structures present. These defect structures have several origins including the drying process of the protein on the stamp and the peeling process of stamp removal during transfer of the protein layer to the substrate [33]. The lanes are stable under SFM imaging in air for multiple frames at low magnification. However, at higher resolution, increased scan forces and contact times tend to disrupt the films.

The measured lane height when imaged in PBS ($h_{PBS} = 12$–14 nm) was much greater than that observed for the same structures in air (Fig. 4A). This result suggests that either the protein layer consists of more than a monolayer of transferred protein, or that some fraction of the transferred protein reorients upon hydration to assume a conformation with its long axis perpendicular to the surface. The peeling defect structures are not as easily resolved once the patterns are placed under fluid due to reduced resolution on the soft, re-hydrated layers.

The BSA pattern displayed a larger height over the reference region even following equilibration with 1 mg/ml HSA for 1 h ($h_{BSA–HSA} = 8$–10 nm). This unexpected result is also supportive of the conclusion that a multiple layer of protein is transferred in the patterned lanes by μCP. Adsorption of the HSA was evident from the morphological changes noted relative to the initial mica lattice.

Following incubation with α-BSA for 1 h, antibody binding was evident on the raised BSA regions while no binding was observed in the intermediate HSA regions. This result indicated that

SFM could be used to distinguish patterned antigen arrays via antibody binding given sufficient height contrast (e.g. > 3 nm in this study). We observed the antibody–antigen binding to be non-uniform. This behavior could be due to masking of the antigenic sites in the patterned molecule aggregates that are non-recognizable due to denaturation or disruption of the antibody–antigen complexes under the lateral scan forces of the SFM tip.

OPN is a slightly smaller protein than BSA (40 kDa compared to 66 kDa for BSA), that plays a prominent functional role in wound healing. Standard glass slides, pre-adsorbed with a monolayer of BSA, were patterned with an overlayer of OPN via μCP (10 μm holes). Fig. 5A displays an SFM topograph taken in air of the OPN patterned regions surrounding the circular regions of exposed BSA. The OPN layer is 2.5–3.5 nm higher on average than the BSA regions, with many regions of apparent aggregates and defects. The aggregate regions are raised 10–14 nm over the OPN, and 12–18 nm over the BSA level. These observations are consistent with the "aggregate" feature noted for adsorbed antibodies on microtitre plates [33]. In addition, similar behavior has been described for μCP poly(ethylene imine) (PEI) [34]. For this polymeric system, the mechanism of defect induction was hypothesized to be dewetting of the thin film on the PDMS stamp surface. Larger heights are noted for apparent peeling defects. Only those regions contacted by the stamp display the aggregate transfer and defect structure. Fig. 5B displays the corresponding fluorescence microscopy image from a patterned OPN surface following primary antibody interaction and secondary labeling. The BSA regions are strongly non-fluorescent, while the OPN regions display both an increased background fluorescence and a more intense, mottled, non-uniform fluorescence pattern. The background fluorescence arises from the well transferred OPN that retains its bioactivity and successfully binds the primary antibody. The mottled non-uniform fluorescence pattern arises from the increased localization of OPN, α-OPN, and α-goat around aggregation points of OPN and defect sites. The addition of the antibodies led to increased feature heights observed with the SFM ($+$ 20–30 nm), which is greater than expected for a single antibody binding.

This result is attributed to the fact that repeated washing and drying steps may lead to surface tension induced protein aggregation and increased surface heights. We observed similar rinse/dry related artifacts in other μCP protein patterns (including BSA), both when dried on the stamp, and when rinsed on the substrate surface. It is important to note the utility of parallel SFM and fluorescence microanalysis to determine the origin of such artifacts.

Quantification of the binding forces between the α-OPN and μCP OPN surfaces was attempted. The α-OPN was attached to the SFM tips via a two-step thermochemical and photochemical conjugation scheme. This scheme was employed for its versatility, and stable covalent coupling of the protein to the probe surface. Crucial to the success of this approach is the creation of a well-formed silane film on the tip. SFM of flat silicon control surfaces treated in parallel indicated a smooth surface film with a roughness of 1.05 nm, and some discrete islands 4–5 nm in height. ESCA analysis (Fig. 6) indicated a large increase in the carbon and nitrogen signals over the silicon control consistent with the formation of an aminated silane overlayer. Furthermore, the chemical shift of the carbon 1s spectra clearly reflected the presence of $\underline{C}$-NH-C and $\underline{C}NH_2$ species arising from the ethylenediamine functionality ($-CH_2CH_2NHCH_2CH_2NH_2$). Some $\underline{C}NO$ species were noted, indicating some loss of reactive amine during handling.

OPN was patterned onto mica and imaged under buffer (PBS, pH 7.4, 150 mM NaCl). The resolution of the protein lane was reduced relative to that observed with the unfunctionalized tips, indicating an increase in tip radius and the presence of a soft compliant layer on the tip surface. Force curves at multiple spots were acquired in both the OPN and mica regions. Movement from spot to spot was performed with the tip retracted out of contact, but with feedback on, and all force curves were taken with the lateral scanning off (scan size $= 0$ nm).

Fig. 7 displays a typical set of retraction (adhesion force) curves between the α-OPN tip and the two surface regions. The OPN/α-OPN interaction

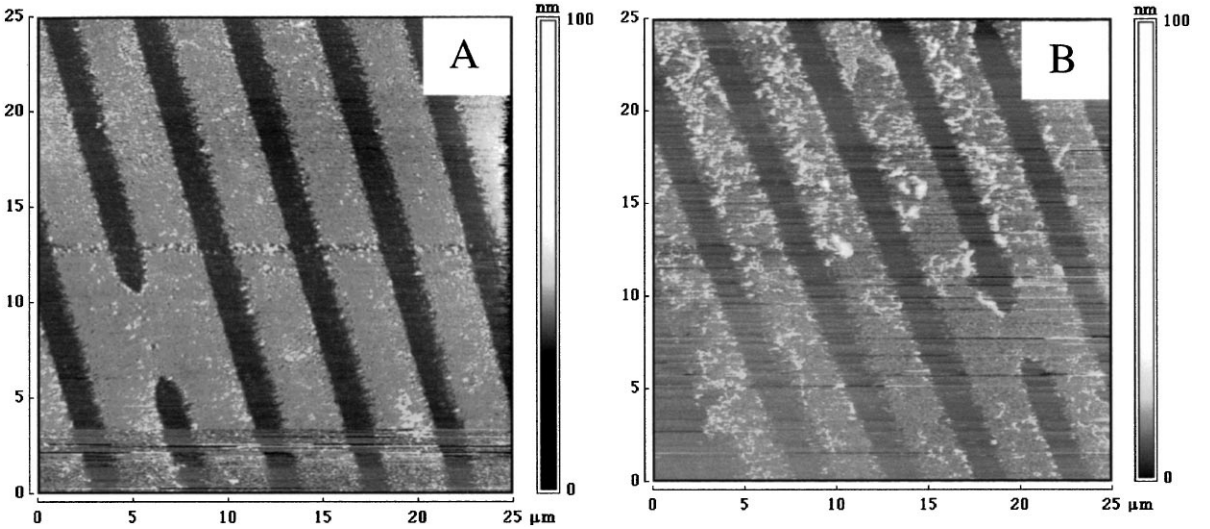

Fig. 4. μCP BSA and antibody recognition. (A) SFM image of a 2 μm μCP line pattern of BSA on mica (μCP as in Fig. 3). Imaged in PBS (pH 7.4, 150 mM NaCl) with an oxide sharpened tip. A large stamp defect of two collapsed lanes is observed. A tip-induced defect from the initial touchdown scan line is noted in the center of the image. The load during imaging was reduced to the lowest value possible for resolution of surface features ($\approx$ 200 pN). (B) SFM image of another spot on the 2 μm line pattern following sequential incubation with human serum albumin (HSA, 1 mg/ml in PBS, 1 h followed by 60 $\times$ volume flushing of the fluid cell) and α-BSA (α-BSA, 100 μg/ml in PBS followed by 60 $\times$ volume flushing of fluid cell). The antibody binding to the BSA lanes is evident from the raised topography.

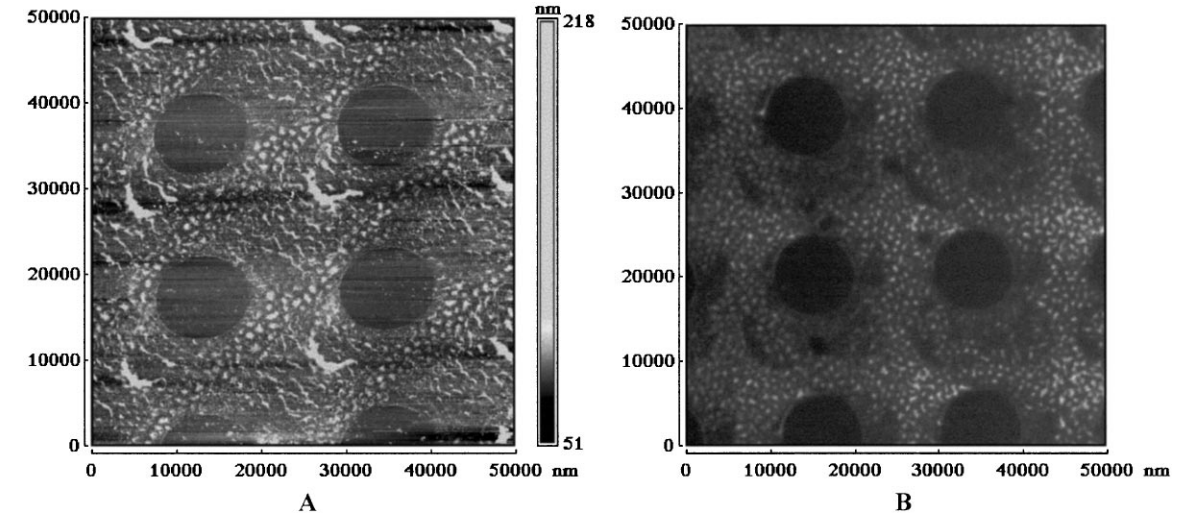

Fig. 5. OPN patterning. (A) SFM image of osteopontin protein patterned (10 μm holes) via μCP on a monolayer of BSA adsorbed on glass. Contact time of 1 min, 100 μg/ml OPN in PBS inking solution. Imaged in air with a contact ultrasharp silicon tip. (B) Fluorescence micrograph of a parallel surface as in (A) following incubation with α-OPN (10 μg/ml, 1 h) and α-Goat (1 : 100 dilution, 1 h). The α-goat is FITC labeled. Similar antibody (primary and secondary) images were obtained via SFM imaging in air.

regularly displayed characteristic multiple stepwise features in the jump off, while the mica/ α-OPN interaction did not. In addition, the forces measured to separate the OPN/ α-OPN junction was always much greater than that observed in the mica lanes (Figs. 8 and 9). The unspecific background

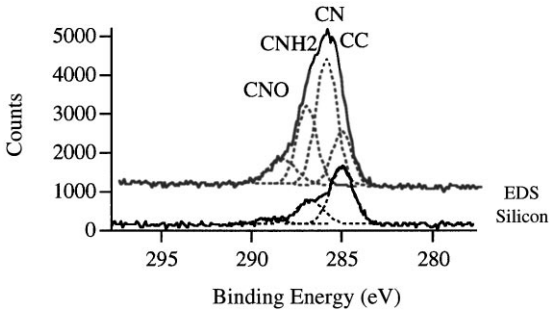

Elemental Composition

	%C	%O	%Si	%N
EDS	29.5	32.5	31.4	6.6
Silicon	9.5	45.4	45.1	0

EDS High-Resolution C1s

	CC	CNC	CNH_2	CNO
actual	18.1	44.1	25.8	12.0
expected	25	50	25	0

Fig. 6. ESCA characterization of EDS surface. High-resolution ESCA of the C1s regions (charge corrected using 285 eV for the hydrocarbon peak) on silicon- and EDS-treated silicon. Each EDS functional group contains two carbon atoms bonded to a secondary amine, and one carbon bonded to the primary amine, as reflected in the spectra. The total surface elemental composition reflects the incorporation of surface carbon and nitrogen, with corresponding loss of signal from silicon and oxygen due to the overlayer formation.

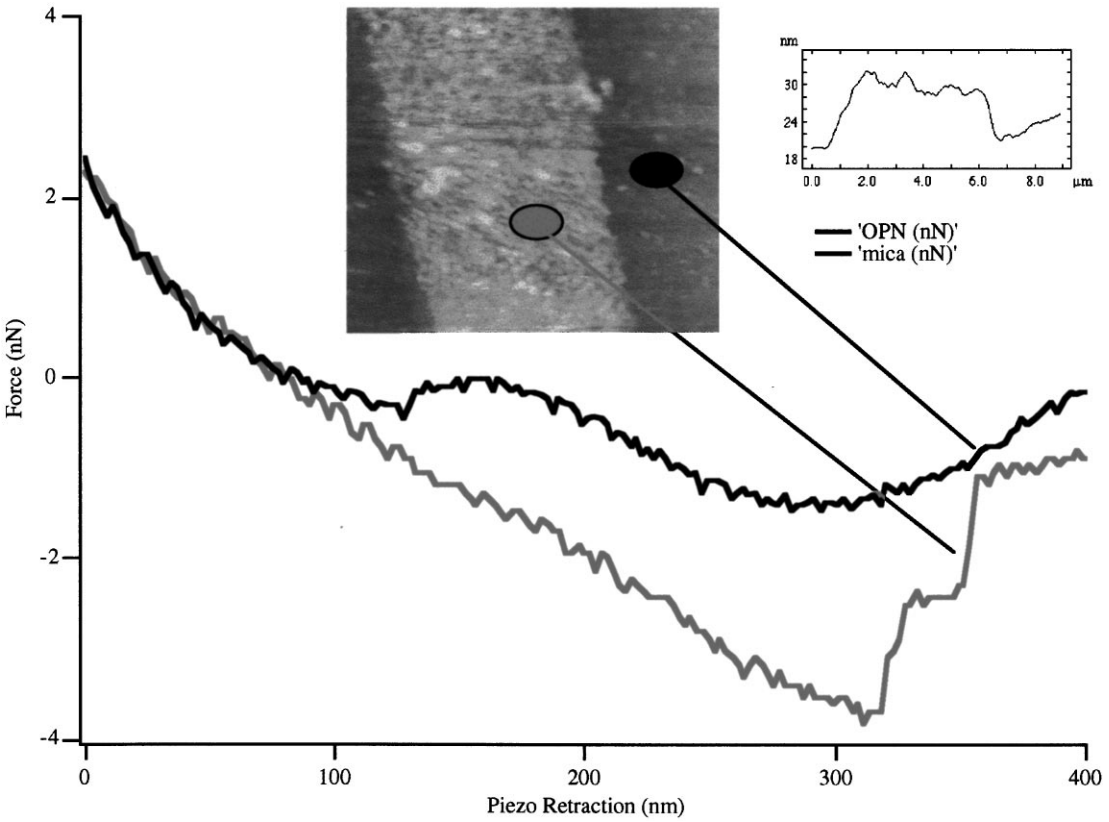

Fig. 7. Representative force curves for an α-OPN tip and an patterned OPN surface in PBS (pH 7.4, 150 mM NaCl): — mica region; — OPN region. Insets display an image of the patterned surface taken with the α-OPN tip, and a line plot across the image to illustrate the lane height (h_{OPN} = 6–8 nm). The *y*-axis of the force plot was converted from deflection using the sensitivity constant of the photodiode and the cantilever force constant.

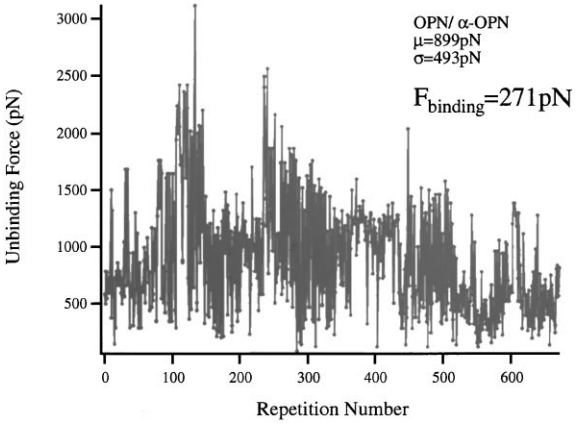

Fig. 8. Plot of the discrete OPN/α-OPN unbinding events. Measured from force curves taken at various spots on OPN lanes. Using a Poisson statistical treatment of the data ($F_{\text{bind}} = \sigma^2/\mu$), the discrete bond force is calculated to be 271 pN.

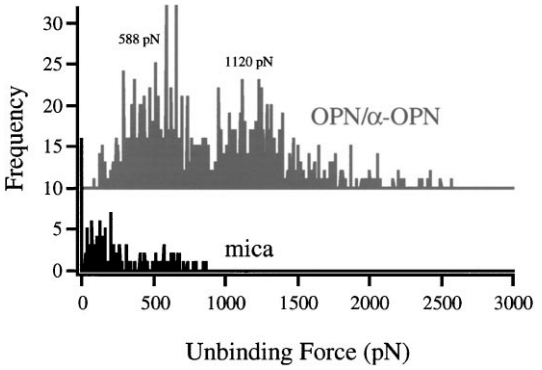

Fig. 9. Histogram plot of the force curve data for the α-OPN tip on the OPN and mica lanes. Using a histogram representation, it appears that the distribution does not follow a single Poisson model. Rather, two sub peaks exist with mean forces of 588, and 1120 pN (Gaussian fit to the data).

noise measured from the scope traces was 51 pN (rms).

Plotting the set of force curves from the osteopontin lane as a function of repetition number, the unbinding force ranged from 40 to 2600 pN (Fig. 8). Initially, it was expected that the unbinding statistics would follow a Poisson distribution [35–37], therefore the data was analyzed in this manner. With Poisson distributions, the discrete quantized single binding event can be mathematically determined from the ratio of the variance to the mean of the distribution. This analysis method resulted in a quantized antibody–antigen recognition event of 271 pN. This unbinding force value is consistent with that reported in the literature for antibody–antigen binding systems (49–244 pN) [13,17,18,21]. In the force curve example displayed in Fig. 7, this value also indicates that each discrete force step noted in the retraction curve would arise from approximately 5–6 binding events.

However, a histogram of the data indicates that the distribution is not a simple, single Poisson distribution (Fig. 9). Rather it appears that multiple distributions are present in the separation events. A critical assumption in the use of the Poisson statistical approximation for determination of discrete bond values is that all discrete unbinding forces must be identical, otherwise multiple distributions will be averaged by the statistical treatment. In the case of weakly associating polyclonal antibody–antigen complexes, different epitopes give rise to different affinities, therefore binding would result in a range of pull-off forces. Partial denaturation of the OPN might also lead to a broadening of the force distribution. Furthermore, as the OPN is not covalently bound to the substrate, each tip–sample separation may contain some mica/OPN non-specific separation. The multiple distributions in the histogram may therefore contain multiple unbinding events, and the actual discrete bond force would then be a sub-multiple of the 588, 1120 pN distribution series. To discriminate and separate the influences of the many possible interactions, control experiments involving non-immune antibody binding, and addition of soluble blocking agents to the fluid cell medium are required. Current efforts in our lab are focused in this area.

4. Conclusions

This work describes the use of SFM to quantitatively interrogate patterned biomolecules. The cantilever force constant was accurately determined via the thermal noise method and bandwidth modification of the microscope. Surface patterns of proteins were fabricated using μCP. Incorporation of

the pattern greatly facilitated visualization of the surface engineering phenomena and subsequent biorecognition via SFM and fluorescence microscopy by providing an internal control element. Osteopontin, a molecule of interest in wound healing and the direction of biological response, was patterned using μCP. Recognition between a patterned OPN surface and OPN antibody could be laterally visualized via SFM topography, or quantified via discrete force curve analysis. This work represents a significant step on the path to developing the SFM as a tool for the engineering of biomaterial surfaces for the direction of biological response.

Acknowledgements

This work was supported by UWEB (University of Washington Engineered Biomaterials, NSF grant EEC 9529161), and the National ESCA and Surface Analysis Center for Biomedical Problems (NESAC/BIO NIH NCRR grant RR01296). Dr. Giachelli is an Established Investigator of the American Heart Association.

References

[1] M. Gerritsen, J.A. Jansen, A. Kros, R.J.M. Nolte, J.A. Lutterman, J. Invest. Surg. 11 (3) (1998) 163.
[2] B.D. Ratner, J. Mol. Rec. 9 (5–6) (1996) 617.
[3] J.H. Brauker, V.E. Carr-Brendel, L.A. Martinson, J. Crudele, W.D. Johnston, R.C. Johnson, J. Biomed. Mat. Res. 29 (1995) 1517.
[4] L. Martinson, personal communication, 1999.
[5] B.D. Ratner, J. Biomed. Mater. Res. 27 (7) (1993) 837.
[6] L.L. Hench, Biomaterials. 19 (16) (1998) 1419.
[7] S.H. Gellman, Chem. Rev. 97 (5) (1997) 1231.
[8] R.E. Babine, S.L. Bender, Chem. Rev. 97 (5) (1997) 1359.
[9] G. Binnig, C.F. Quate, C. Gerber, Phys. Rev. Lett. 56 (9) (1986) 930.
[10] J.H. Hoh, J.P. Cleveland, C.B. Prater, J.-P. Revel, P.K. Hansma, J. Amer. Chem. Soc. 114 (1992) 4917.
[11] G.U. Lee, D.A. Kidwell, R.J. Colton, Langmuir 10 (1994) 354.
[12] E.-L. Florin, V.T. Moy, H.E. Gaub, Science 264 (1994) 415.
[13] P. Hinterdorfer, W. Baumgartner, H.J. Gruber, K. Schilcher, H. Schindler, Proc. Natl. Acad. Sci. USA 93 (1996) 3477.
[14] M. Ludwig, W. Dettmann, H.E. Gaub, Biophys. J. 72 (1997) 445.
[15] V.T. Moy, E.-L. Florin, H.E. Gaub, Science 266 (1994) 257.
[16] A. Chilkoti, T. Boland, B.D. Ratner, P.S. Stayton, Biophys. J. 69 (1995) 2125.
[17] S. Allen, X. Chen, J. Davies, M.C. Davies, A.C. Dawkes, J.C. Edwards, C.J. Roberts, J. Sefton, S.J.B. Tendler, P.M. Williams, Biochem. 36 (24) (1997) 7457.
[18] U. Dammer, M. Hegner, D. Anselmetti, P. Wagner, M. Dreier, W. Huber, H.J. Güntherodt, Biophys. J. 70 (1996) 2437.
[19] T. Boland, B.D. Ratner, Proc. Natl. Acad. Sci. USA 92 (1995) 5297.
[20] G.U. Lee, L.A. Chrisey, R.J. Colton, Science 266 (1994) 771.
[21] O. Willemsen, M.M.E. Snel, K.O. van der Werf, B.G. de Grooth, J. Greve, P. Hinterdorfer, H.J. Gruber, H. Schindler, Y. van Kooyk, C.G. Figdor, Biophys. J. 75 (1998) 2220.
[22] P. Hinterdorfer, K. Schilcher, W. Baumgartner, H.J. Gruber, H. Schindler, Nanobiology 4 (1998) 177.
[23] C.J. Roberts, S. Allen, X. Chen, M.C. Davies, S.J.B. Tendler, P.M. Williams, Nanobiology 4 (1998) 163.
[24] C.D. James, R.C. Davis, L. Kam, H.G. Craighead, M. Issacson, J.N. Turner, W. Shain, Langmuir 14 (4) (1998) 741.
[25] A. Bernard, E. Delamarche, H. Schmid, B. Michel, H.R. Bosshard, H. Biebuyck, Langmuir 14 (9) (1998) 2225.
[26] X.-M. Zhao, Y. Xia, G.M. Whitesides, J. Mater. Chem. 7 (7) (1997) 1069.
[27] D.T. Denhardt, M. Noda, J. Cell. Biochem. Suppl. 30–31 (1998) 92–102.
[28] M.D. McKee, A. Nanci, Conn. Tissue Res. 35 (1–4) (1996) 197.
[29] T. Wada, M.D. McKee, S. Steitz, C.M. Giachelli, Circ. Res. 84 (1999) 166.
[30] L. Liaw, M. Almeda, C.E. Hart, S.M. Schwartz, C.M. Giachelli, Circ. Res. 74 (1994) 214.
[31] J.L. Hutter, J. Bechhoefer, Rev. Sci. Inst. 64 (7) (1993) 1868.
[32] J.P. Cleveland, personal communication, 1997.
[33] J. Hayes, M. Kenmore, A. Badley, D.C. Cullen, Nanobiology 4 (1998) 141.
[34] L. Yan, W.T.S. Huck, X.M. Zhao, G.M. Whitesides, Langmuir 15 (4) (1999) 1208.
[35] T. Han, J.M. Williams, T.P.J. Beebe, Anal. Chim. Acta. 307 (1995) 365.
[36] J.M. Williams, T. Han, T.P.J. Beebe, Langmuir 12 (1996) 1291.
[37] L.A. Wenzler, G.L. Moues, G.N. Raikar, R.L. Hansen, J.M. Harris, T.P.J. Beebe, L.L. Wood, S.S. Saavedra, Langmuir 13 (14) (1997) 3761.